Universidad Zaragoza

1542

Final Master Project

Oriented functionalization of magnetic nanoparticles with E-cadherin

Author

Eduardo Moreno Antolín

Supervisors

Dr. Raluca M. Fratila

Dr. Valeria Grazú

Master in nanostructured materials for nanotechnological applications

2017-2018

Abbreviations

AMF: Alternating Magnetic Field

BBS: Borate buffered saline

DLS: Dynamic Light Scattering

DMEM: Dulbecco's Modified Eagle's Medium

ECs: cadherin domains

E-cad: E-cadherin (EC1-2), histidine tagged.

EDC: 1-ethyl-3-(3-dimethylaminopropyl)carbodiimide

EDTA: Ethylenediaminetetraacetic acid

EMT: Epithelial-Mesenchymal Transition

FBS: Fetal Bovine Serum

IPTG: isopropyl β-D-1-thiogalactopyranoside

LB: Lysogeny Broth

MES: 2-(*N*-morpholino)ethanesulfonic acid

MNPs: Magnetic Nanoparticles

MW: Molecular Weight

NTA: N_{α},N_{α}-Bis(carboxymethyl)-L-lysine hydrate

OD: Optical Density

PBS: Phosphate Buffer Saline

PEG: polyethylene glycol

PMAO: poly(maleic anhydride-*alt*-1-octadecene)

TAMRA: tetramethylrhodamine-cadaverine

TB: Terrific Broth

TEM: Transmission Electron Microscopy

TGA: Thermogravimetric Analysis

TRIS: Tris(hydroxymethyl)aminomethane

S-NHS: *N*-Hydroxysulfosuccinimide

SDS-PAGE: denaturizing polyacrylamide gel electrophoresis

Abstract

The synergy between nanotechnology and biological science is being exploited in the last years, giving rise to a great amount of knowledge generation and applications in a wide variety of fields. This increasing use of this type of nano-sized materials has awakened the interest on the interaction between them and biological entities: cells, tissues or organisms. Among all the types of available nanomaterials, iron oxide magnetic nanoparticles have shown a huge potential in the biomedical field due to their biocompatibility and other interesting properties, especially their ability to produce heat when exposed to an external alternating magnetic field. A virtually unexplored subject is the interaction of magnetic nanoparticles with cell membranes of living cells. The study of this topic will have impact on fundamental science (i.e. biophysical studies of the cell membrane under localized heating, changes in heating efficiency of nanoparticles when interacting with living cells) and will allow the development of brand new applications (i.e. hyperthermia treatment, cell transfection).

In the work here presented, E-cadherin has been selected as a targeting agent. It is a ubiquitous adhesion protein present in the cell membranes of many cell types, with important physiological functions and a key role in cancer progression. Spherical magnetic nanoparticles have been functionalized with this protein in an oriented manner, so that they are able to interact with the homologue proteins in the cell membrane. In that way, this is proposed as an approach to immobilize magnetic nanoparticles on the cells surface. Two different strategies were designed, one of them showing promising results of the oriented functionalization. However, the efficiency of the process needs to be further optimized for the future applications of this platform.

Resumen en español para público no científico

Actualmente, nanotecnología y biotecnología son dos disciplinas en auge que aportan importantes contribuciones a la ciencia y la sociedad. Más allá de sus aportaciones por separado, estas dos áreas de conocimiento presentan una gran sinergia cuando se combinan. La nanotecnología trabaja con materiales con un tamaño muy reducido: en el orden de los nanómetros, 100.000 veces más pequeños que el grosor de un pelo. Este tamaño nanométrico otorga a materiales ampliamente conocidos (como el oro o la magnetita) nuevas propiedades que no poseen cuando se encuentran con tamaño macroscópico. Las nanopartículas de oro, por ejemplo, poseen distintos colores dependiendo de su tamaño (siempre en el rango de nanómetros), muy distintos al habitual dorado. Así, algunas propiedades emergentes pueden ser aprovechadas para distintas aplicaciones. En el caso de las nanopartículas magnéticas de óxido de hierro, que podrían considerarse diminutos imanes, son capaces de producir calor de manera local cuando se les expone a un llamado campo magnético alterno, que actúa sin entrar en contacto físico con las nanopartículas. Esto permite aplicaciones como la eliminación de células tumorales mediante un calentamiento muy localizado utilizando estas nanopartículas magnéticas, con una activación externa y no invasiva. Esto además reduciría los efectos secundarios al minimizar el daño a tejidos sanos.

Por esta aplicación explicada y otras de diferentes índoles, resulta interesante conseguir que estas nanopartículas magnéticas se unan específicamente a las células que nos interesen. Este trabajo se centra en conseguir *decorar* las nanopartículas con lo que denominaremos *piezas de puzle* que les permitan encajar y unirse a sus complementarias, que estarán presentes en las células. Estas *piezas* deberán estar unidas con una orientación adecuada para que pueda encajar con su contrario, y así conseguir que queden inmovilizadas en las células de una manera específica y localizada, que podrá aprovecharse en el futuro para el desarrollo de aplicaciones tanto para ciencia básica, como para ámbitos biomédicos.

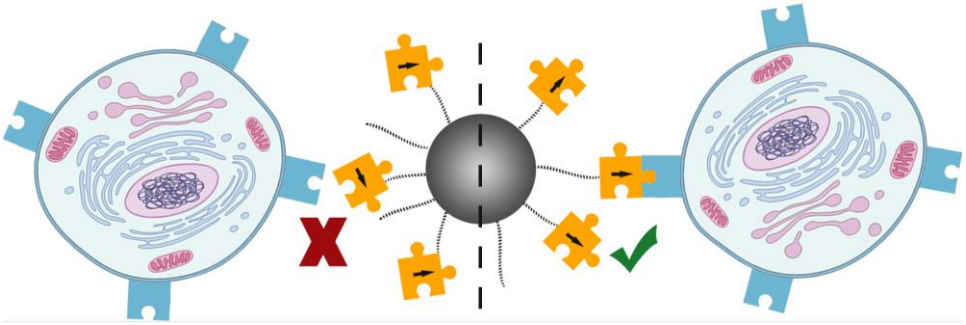

INDEX

1. Introduction

1.1. Nano- and biotechnology

Nanotechnology is perceived as one of the main revolutions of the 21st century. It possesses a huge potential derived from the wide variety of materials and diversity of new properties emerging from the nanoscale dimension.[1,2] The increasing control of the synthesis and functionalization of materials with smaller size broadens the scope of this scientific field, becoming more and more multidisciplinary. One of the main symbiosis – with biological sciences – has given rise to a brand new field, known as bionanotechnology.[3–6] The aim of this area is to use different nanomaterials for all kind of biological applications, from biomedicine and biosensing to industrial biotechnological production. The result of the synergy between both disciplines can be found in a wide range of applications. Food industry has long taken advantage of nanoemulsions[7], and medicine has plenty of examples in which nanotechnology is involved, especially in cancer treatment[8–11]. Fundamental research has also been provided with new tools from the nanotechnology world, such as the atomic force microscopes, that allow the study of biophysical properties of a single biomacromolecule (i.e. a protein)[12] or the formation of artificial monolayers to study the properties of biological membranes[13].

1.2. Magnetic nanoparticles and hyperthermia

Magnetic nanoparticles (MNPs) are composed of a magnetic material (most commonly iron oxide or a doped iron oxide)[14,15] and their size is below 100 nm in all their dimensions. MNPs – and especially those composed of iron oxides, magnetite and maghemite – have an increasing number of applications in the biomedical field due to their biocompatibility, stability, non-toxicity and their superparamagnetism at small sizes.[14,16,17]

One of the most interesting properties of MNPs is their ability to produce heat when exposed to an external alternating magnetic field (AMF), process known as magnetic hyperthermia. In the case of superparamagnetic MNPs, this is mainly due to two mechanisms: Brownian and Néel relaxation. The first one consists of the physical rotation of the nanoparticle to orient towards the direction of the external magnetic field. In the Néel relaxation, the nanoparticle does not move and the magnetic moment itself rotates to orient in parallel with the field direction.[18–20]

Much research has been done focusing on the application of these MNPs in the treatment of cancer as hyperthermia has shown a great potential both alone and in combination with other treatments.[21–26] In fact, most of the applications developed for this type of nanoparticles are related to cancer treatment[27] or drug delivery following different strategies[28].

1.3. Interaction of magnetic nanoparticles with cell membranes

The interaction between nanomaterials and living organisms has long been an area of interest. It stands in a position where fundamental and applied research meet, as the understanding of how a specific nanomaterial interplays with a cell, or how an organism responds to its presence, promotes the appearance of new applications for these nanosized materials. Regarding that, many toxicity studies of MNPs have been performed both *in vitro* and *in vivo*.[28]

Nevertheless, toxicity, although crucial, is not the only aspect worth studying of the relationship between nanomaterials and living systems. The interaction of nanomaterials with the cell membrane is related with the cellular uptake and can trigger signalling processes. Besides, the heating efficiency of MNPs varies when they are interacting with cells. The Brownian relaxation contribution to heat generation decreases dramatically in highly viscous environments or when something (i.e. a covalent bond or the interaction with large biological structures such as the cell membrane) impedes the physical rotation. Therefore, the location of the MNPs – extracellular matrix, cell membrane or cytosol – highly influences the heating efficiency, as Di Corato *et al.* demonstrated in their work with fixed cells.[29] It would be convenient to study the influence of the interaction of MNPs with living cells on their heating efficiency. However, although it is easy to have a model of internalized MNPs, retaining them on the cell membrane is particularly challenging. It is relatively straightforward to functionalize MNPs to target cell membrane receptors (i.e. with antibodies as targeting agents), but the constant renewal and exchange of those biomolecules or a triggered endocytosis can promote MNP internalization sooner than desired.[30,31]

Attaching MNPs to the cell membrane without triggering active uptake mechanisms would not only permit the study of their heating efficiency but would also provide a resourceful tool for other fundamental studies such as biophysical studies of the cell membrane under localized heating. In addition, being able to gain control on the genera-

tion of long-lived hotspots on the membrane could allow the formation of reversible pores, useful for the intracellular delivery of biomolecules such as proteins or DNA – therefore, giving birth to a universal tool for transfection.

Our group is currently working on the immobilization of MNPs on the cell membranes through different strategies. One of the strategies being used to target the cell membrane is focused on the use of covalent chemistry, namely biorthogonal *click* chemistry.[32] In this case, our preliminary result indicate that the probe used to target the cell membrane remains there for approximately 8 hours (J. Idiago-López *et al.*, in preparation), enough time to perform measurements of the effect of the application of an AMF. The work here presented is based on the use of another strategy: non-covalent targeting of the cell membrane involving adhesion proteins, concretely cadherins.

1.4. Cadherins to target the cell membrane

Cadherins constitute a superfamily of cell-adhesion molecules with a crucial role in maintaining cell and tissue structure, and in cellular movement. They are also pivotal in morphogenesis during animal development. Among them, classic cadherins are homophilic Ca^{2+}-dependent cell-cell adhesion macromolecules, and integrate members such as E-, N- and P- cadherins. The extracellular part of these proteins – by which they interact with each other – is spatially structured in five domains (referred to as EC1-5). When adjacent cells contact each other, cadherins from the opposing cells located at the site of contact form *trans*-bonds across the interphase. Once those bonds are arranged, cadherins can regulate the formation of the cell-cell contact in three different ways: by reducing the local interfacial tension directly – through adhesion tension – and indirectly – through signalling towards the actomyosin cytoskeleton, as well as by establishing the mechanical coupling of the contacting cells.[33] On the intracellular part, the cadherin domains interplay with signalling proteins of different pathways: Wnt/β-catenin, Rho-GTPases, citoplasmatic kinases, etc.[34,35] Figure 1 represents a scheme on a tight junction, the role of cadherins and the connection with structural and signalling molecules.

Apart from their function in the mentioned physiological processes, cadherins are important in cancer progression. The epithelial-mesenchymal transition (EMT) is a process through which epithelial cells lose their cell polarity and cell-cell adhesion capacity. When a tumour undergoes the EMT, it transforms from quiescent to metastatic. This is partially due to a change in cadherins expression: E-cadherin (characteristically ex-

pressed in adult organisms) expression decreases and N-cadherin (present only during embryonic development) expression is induced. This switch leads to loosening of intercellular junctions, allowing tumour cells to escape from their original tissue and migrate, originating metastasis.[36]

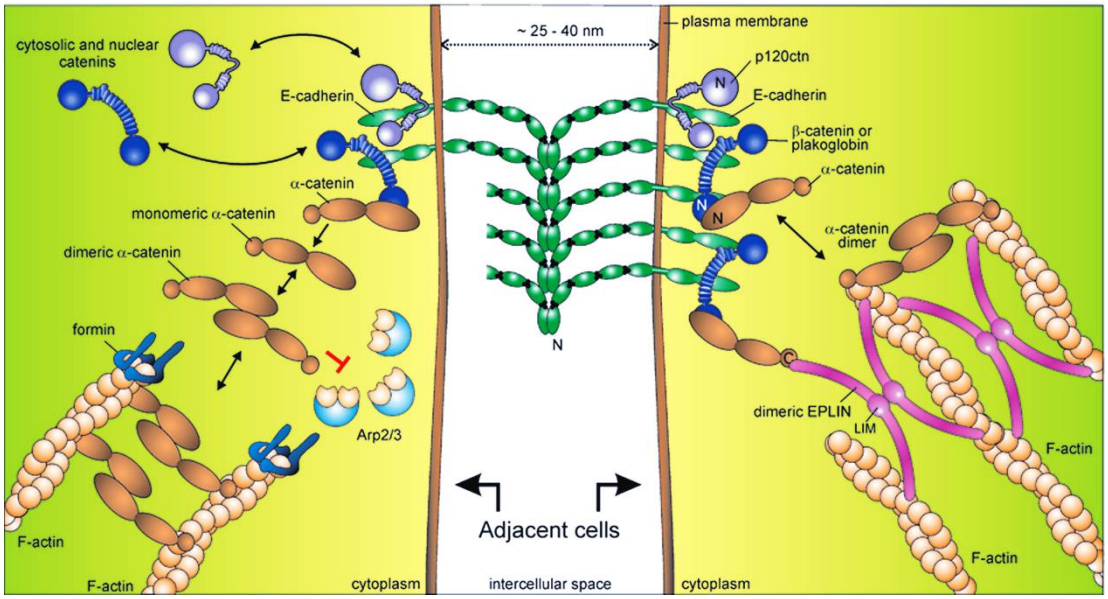

Figure 1. Scheme of a tight junction between two adjacent cells, showing the extracellular interaction of the cadherins and the interplay with the structural and signalling molecule intracellularly. Adapted from Roy and Berx, 2008.

Although cadherins analysis is always present in cancer research, there is no much work taking advantage of their spatial location within cells to target the cell membrane. Some studies show the loading of polymeric nanoparticles with vascular endothelial cadherin for anticoagulation purposes[37], use aptamers of E-cad to deliver drugs[38], or functionalize MNPs with anti-cadherin 11 antibodies as immunotargeting[39]. The latter strategy resembles the concept of the present work.

Our idea of attaching MNPs to the cell surface requires targeting a ubiquitous molecule. In this sense cadherins fulfilled this requirement. However, there are multiple classes of cadherin molecules: classical (type I and II), desmosomal, seven-pass transmembrane, large cadherins of the fat and dachsous group and protocadherins.[35] Cells containing a specific cadherin subtype tend to cluster together by homophylic interaction excluding cells containing other cadherin subtypes.

Particularly, in our work we have focused our efforts on the development of MNPs for targeting E-cadherin expressing cells. E-cad is one of the first characterized cadherins. It is the prototype of type I classical cadherins, group where N- and DE-cadherin

can also be found. Therefore, it presents most of the properties and characteristics mentioned when the whole family was presented. Many studies have enlightened the structure, the transcript processing, function, signalling pathway involved, etc.[40]

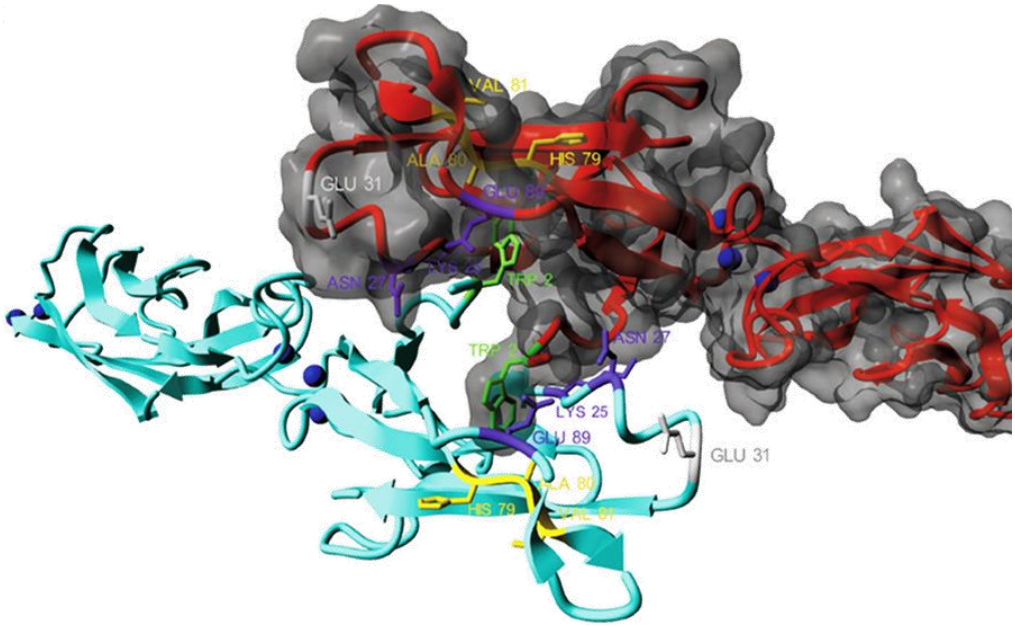

Figure 2. Model interaction of two human E-cad EC1-2 domains (PDB 2O72). Blue dots are Ca^{2+} ions. Adapted from Roy and Berx, 2008.

As our objective is to mimic the homophylic interaction between two E-cad expressing cells for ensuring a long-live attachment of MNPs to the cell membrane, it is crucial to understand the interaction between two E-cad molecules. As it is shown in Figure 2, this interaction is Ca^{2+}-dependant and takes place between the two outer domains of the N-terminal (EC1-2) of each identical protein.[35,40] Previous work have shown that the use of recombinant fragments containing this two outer domains (EC1-2) is enough to establish stable homophylic interactions between microspheres and surfaces functionalized with E-cadherin fragments.[41,42] Besides, unpublished previous results of Helene Feracci (collaborator of our group) showed that by using EC1-2 mutants (W2A) it is possible to target E-cadherin expressing cells while avoiding the internalization of the targeting particle.

All these previous results encouraged us to optimize the functionalization of magnetic nanoparticles with E-cad EC1-2 recombinant fragments with the ultimate goal of generating long-lived hotspot at the cell membrane triggered by AMF. However, this is a challenging task, as it would be necessary to ensure an oriented binding of the frag-

ments as well as to achieve a multivalent binding to the target cells and colloidal stability of the functionalized MNPs in cell-culture media.

As the interaction between two E-cad depends on a correct spatial position, the orientation of the protein domains on the nanoparticle surface is crucial for a correct attachment to the cell membrane. In general, the random functionalization – that is, with no control of the orientation – of nanoparticles with proteins is straightforward. However, the difficulty increases when the position or orientation of the biomolecule is important for the application. Studies where cadherins are used to target cells are based on the random functionalization of microspheres[41,43] because the contact surface between the cell and the microparticle is larger. Therefore, there will be statistically enough protein molecules with the correct orientation to establish the binding. However, nanoparticles show a dramatically smaller contact area, so it is logical to assume that a good orientation of all the molecules is required to ensure a multivalent union that secure the binding to the cell membrane. The adhesion junction of cells is composed by interspaced clusters of less than ten cadherin molecules (with a median of 6).[44]

A similar challenge has been encountered for the functionalization of nanoparticles with antibodies. In this case, modifying the pH conditions during the functionalization can help to obtain the desired orientation due to ionic interactions previous to the covalent binding. Thus, the availability of the antigen-recognition domain increases.[39,45] In the present work, due to the small size of the recombinant cadherin fragments, a more universal strategy is needed. A widespread methodology in the protein research field is the metal-chelate affinity chromatography, generally applied to resins, surfaces and big polymeric microbeads. Here we adapt this procedure to functionalize MNPs with oriented and immobilized E-cadherin. This work uses a nitrilotriacetic derivative, N_α,N_α-Bis(carboxymethyl)-L-lysine hydrate (in this manuscript, abbreviated as NTA), to functionalize the MNPs surface. NTA is able to chelate divalent cations such as Cu^{2+}, Ni^{2+}, Zn^{2+} or Co^{2+}, which at the same time will be able to chelate the histidines of the His-tag of a recombinant protein.[46–48] As we have the EC12 fragments cloned in a pET plasmid that introduced a His-tag at the C-terminal end of the fragment, we could use this strategy to ensure their oriented binding to the MNPs. Although this strategy has been used in different occasions with other nanoparticles showing promising results[49–51] it has never been tested with MNPs that have a natural tendency to aggregate due to magnetic attraction.

2. Objectives

The general objective of this work is to optimize the oriented binding of EC1-2 cadherin fragments to MNPs through the metal-chelation to the His-tag sequence fused in their C-terminus. To achieve this goal, the following specific objectives were established:

1. Synthesis, water transfer and characterization of magnetic nanoparticles.
2. Expression and purification of recombinant E/EC1-2 cadherin fragments.
3. Oriented functionalization of magnetic nanoparticles with E-cadherin fragments.
4. Characterization and analysis of the functionalization.

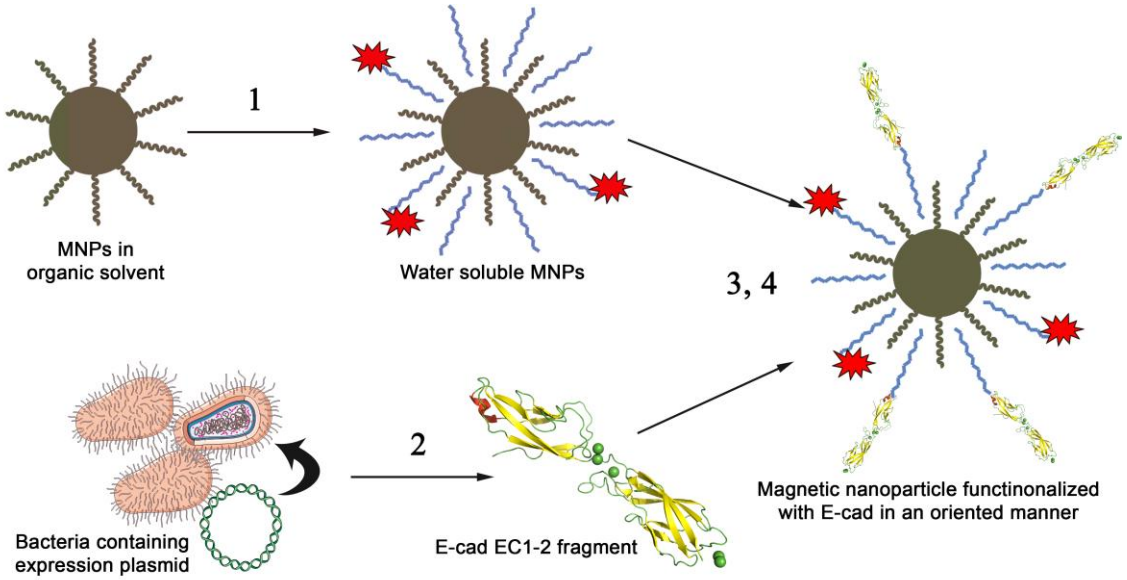

Scheme 1. Objectives of the project.

3. Experimental section

3.1. E-cadherin fragments (EC1-2) production

3.1.1. E-cadherin (EC1-2) expression

100 mL of Lysogeny Broth (LB) medium with kanamycin (50 μg/mL) were used to start a preculture of *Escherichia coli* BL21 containing a pET plasmid with the E-cadherin EC1-2 gen (the two outer domains) and a histidine tag at the C-terminal end. The plasmid was gifted by Dr. Helene Feracci. This was incubated at 37 ºC and under agitation overnight. The next day, a larger culture of 250 mL was prepared, this time with Terrific Broth (TB) medium, diluting the first one to get a final optical density (OD) of 0.1. The culture was incubated at 37 ºC, and when the culture reached an OD of 0.6, the inducing agent of the expression was added, isopropyl β-D-1-thiogalactopyranoside (IPTG). After 2 h of incubation, the culture was centrifuged at 500 xg for 20 min, at 4 ºC. The supernatant was discarded, and the pellet frozen until the extraction of the protein.

3.1.2. E-cadherin extraction and purification

E-cadherin expressed in *E. coli* forms inclusion bodies, so in order to extract and purify the protein, it was denaturalized with urea and renaturalized again by slowly removing the denaturizing agent. The lysis buffer is composed by urea (4 M), Na_2HPO_4 (50 mM), imidazole (20 mM) and β-mercaptoethanol (20 mM) and a protease inhibitor (Protease Inhibitor Cocktail for use in purification of Histidine-tagged proteins, DMSO solution; Ref: P8849-1ML). The pellet obtained from the E-cad expression was resuspended in the lysis buffer in an ice bath (to better inhibit the protease activity) and incubated at 4 ºC for 20 min under light magnetic agitation. The suspension was then centrifuged (10,000 xg, 30 min), and the pellet discarded.

To purify the protein, it was attached to agarose beads with NTA-Ni^{2+} (QIAGEN, Ref. 30430) on the surface. This allowed the specific union of the histidine tags. The beads were washed twice with the urea buffer (lysis buffer without the protease inhibitor), and twice with the lysis buffer. Then, then supernatant of the protein extraction was incubated with the beads (6 mL of agarose beads per 250 mL of bacteria culture) for 2 h, at 4 ºC in a rotating wheel. After that, the beads were centrifuged (3000 xg, 15 min), the supernatant discarded, and the beads washed six times with urea buffer. The result-

ing beads were dialysed against a decreasing urea gradient: 3 M, 2 M, 1 M, and finally several dialysis steps with PBS + β-mercaptoethanol were performed. This slow decrease in urea concentration allows the protein to fold correctly. The beads with the E-cad were stored at 4 ºC in PBS buffer with 0.05% sodium azide to avoid microorganisms or fungus growth (a total volume of around 20 mL).

3.1.3. Trypsin sensitivity assay

When E-cad (EC1-2) is correctly folded, it presents resistance towards trypsin cleavage when there is Ca^{2+} present in the media due to structural modifications. However, in absence of calcium ions, it is susceptible to proteolysis. This is more detailed in the "Results and discussion" section.[52]

Procotol

The amount of agarose beads containing 30 μg of E-cad fragments were washed in buffers containing $CaCl_2$ (presence of Ca^{2+}) or EDTA (absence of Ca^{2+}). Then, the protein was eluted with imidazole (0.25 M) and each sample incubated with trypsin-agarose (Sigma, T4019-50UN). After 1 h of incubation at 37 ºC, the trypsin-agarose was removed through a miniSpin column filter, and the resulting samples loaded in a SDS-PAGE.

3.2. Nanoparticle synthesis and characterization

3.2.1. Water transfer of hydrophobic MNPs

The fundamentals of this step will be further explained in the "Results and discussion" section.

Protocol[32,53]

140 mg of PMAO (MW: 30-50 kDa) were dissolved in 15 mL of $CHCl_3$ in a 500 mL flask. Afterwards, 2 mg of TAMRA dissolved in 2 mL ethanol were added, and the reaction was kept overnight in the dark, under magnetic stirring. The next day, the equivalent to 10 mg of iron in MNPs, dispersed in organic media were washed three times with ethanol using a permanent magnet. After the last washing step, the MNPs were dispersed in 2 mL $CHCl_3$. To the previously prepared PMAO-TAMRA solution, 81 mL of $CHCl_3$ were added, and the MNPs were added drop-wise in an ultrasound bath, achieving a final volume of 100 mL. In this step, the polymer coats the MNPs through

the hydrophobic interactions between the aliphatic chains of the PMAO and the oleic acid ligands present on the MNP surface.

The most part of the organic solvent was removed using a rotary evaporator at 40 ºC and 200-400 mbar. 5-10 mL were left, to which 15 mL of deionized water and 15 mL of NaOH (0.1 M) were simultaneously added. The hydrolysis of the anhydride groups of the PMAO results in carboxyl groups that stabilize the MNPs in aqueous media. The remaining organic solvent was further removed in the rotary evaporator at 70 ºC and 200 mbar. The resulting MNPs suspension was filtered using 0.2 μm filters to eliminate polymer and MNPs aggregates. Finally, the excess of polymer not bound to the MNPs was eliminated by four ultracentrifugation steps at 70,000 xg for 2 hours each; the first two at room temperature, the following ones at 14 ºC.

3.2.2. Iron concentration determination

The reactions, functionalizations and experiments using MNPs were performed by iron mass. Therefore, after each step, the iron concentration had to be determined.

Protocol

The iron concentration was obtained by a spectrophotometric method using Tiron (1,2-dihydroxybenzene-3,5-disulphonic acid). This molecule forms a complex with iron that absorbs light at 480 nm. A calibrating curve was performed with Fe(III) solutions of known concentrations (0, 100, 200, 400, 600 and 800 μg/mL). For the preparation of the MNP samples, 5 μL of MNP suspension were diluted in 45 μL of milliQ water or hexane, depending on their hydrophilic or hydrophobic behaviour. All samples were treated in triplicate.

50 μL of each sample were transferred to Eppendorf tubes and each sample was incubated with 100 μL of aqua regia ($HCl:HNO_3$, 3:1) for 15 min at 60 ºC in order to dissolve the iron of the MNPs. Afterwards, 350 μL of milliQ water were added to stop the reaction, and 50 μL of each solution were transferred to a 96-well plate. To each well, 100 μL of Na_3PO_4 (0.2 M, pH 9.7) and 60 μL of a solution of 50 μL KOH (4M) and 10 μL Tiron (0.25M) previously prepared were added. The plate was incubated for 15 min at room temperature, and the absorbance at 480 nm measured later.

3.2.3. Electrophoresis in agarose gels

Electrophoresis allows the identification of charge and mass changes that MNPs undergo, as less free carboxyl groups remain after each functionalization step. Besides, this technique is also useful for visualizing the unbound polymer in the water transfer step by loading the supernatants from each washing step.

Protocol

1% (m/v) agarose gels were prepared using a tris(hydroxymethyl)aminomethane (TRIS), borate, EDTA (TBE) 0.5X buffer. Samples were mixed with loading buffer: glycerol 25% in TBE (0.5X). The total volume loaded in each well was 8 μL, and the ratio sample:buffer varied according to the concentration of the sample. The electrophoresis was set at 90 V, 45 min.

3.2.4. Thermogravimetric analysis

Thermogravimetric analysis (TGA) is a technique that measures the weight difference of a sample as the temperature increases in a controlled atmosphere. It allows to detect the weight variation that usually occurs in reactions such as decompositions, sublimations, reductions, desorption, absorption, etc. With this methodology, the organic coating of the MNPs can be quantified, and the number of carboxyl groups per nanoparticle can also be estimated.

Protocol

A *Universal V4.5A TA Instrument* equipment was used for the measurements of weight against temperature. The quantification of organic material loss was performed by heating the samples in air, increasing the temperature at a rate of 10 ºC/min until a final temperature of 800 ºC. Organic samples were previously dried in air, and aqueous samples were freeze dried.

3.2.5. Transmission Electron Microscopy (TEM)

A *Tecnai T20 (FEI)* was used, with a thermoionic emission gun and operating at a voltage of up to 200 kV (*Laboratorio de Microscopías Avanzadas*, University of Zaragoza). For the visualization, the sample is prepared over a copper grid covered with carbon (Electron Microscopy Sciences). 5 μL of the sample – previously diluted – are de-

posited on the grid and left to dry in air. Size distribution was analysed with ImageJ software.

3.2.6. Dynamic Light Scattering (DLS)

Dynamic Light Scattering is a spectroscopic technique used to measure the hydrodynamic diameter of molecules, particles or colloids in solution. The samples were prepared in water at a final concentration of 0.05 mg Fe/mL, with a final volume of 1 mL. The pH was adjusted to 7 for all samples, and each sample measured 5 times at 25 ºC in a *Malvern Zetasizer* equipment, irradiating the samples with a monocromatic helium-neon laser of 633 nm.

3.2.7. ζ-potential

ζ-potential is a measurement of the surface charge or surface potential of small particles. A laser pierces the centre of the sample and a detector collects the dispersed light at an angle of 13º. The same samples and measurement equipment were used as for the DLS measurement.

3.3. MNPs functionalization strategies

3.3.1. Strategy A

EDC (100 mM) and S-NHS (100 mM) were mixed and incubated for 10 minutes at room temperature under agitation in 2-(*N*-morpholino)ethanesulfonic acid (MES) (50 mM, pH 6.5). 0.33 mg Fe of PMAO-TAMRA nanoparticles were added to the EDC/S-NHS mixture. The volume was adjusted to a final value of 1.2 mL by addition of MES. The samples were incubated for 30 min under agitation. MNPs were dialysed in 400 mL of MES (50 mM, pH 6.5) for 1 h once and then in HEPES (20 mM, pH 8.0) for 1 h twice. Then, 182 nmol of NTA-Cu^{2+} complex were added to the activated MNPs, and incubated for 2 h at room temperature under agitation. Then, the remaining activated carboxyl groups were blocked with 500 nmol of the blocking agent (TRIS or PEG 750, 2000 or 5000 Da) for 45 min. Finally, the resulting MNPs were incubated with E-cad EC1-2 fragments at different ratios. When imidazole was used, the concentration was 0.25 M. Samples were centrifuged for 2 h, 24,700 xg, 4 ºC.

3.3.2. Strategy B

In this strategy, the functionalizations were performed in two steps. First, 1 mg Fe of PMAO-TAMRA nanoparticles were mixed with 22.26 μmol of PEG (750 Da) and 40 μmol of EDC were added twice at time 0 and 30 min of the reaction that lasted 3 h 30 min. Both PEG and EDC were dissolved in Borate buffered saline (BBS) (50 mM, pH 9.0). Then, eight washes using cellulose membranes (Amicon, Millipore, 100 kDa) were performed.

The second functionalization was similar. 0.5 mg of Fe were mixed with 460 nmol of NTA-Cu^{2+} and 20 μmol of EDC were added twice at time 0 and 30 min of the reaction that lasted 3 h 30 min. The volume was adjusted to a final value of 1.2 mL with BBS buffer. The excess of reactants was removed by dialysis against HEPES (20 mM, pH 7.0, 150 mM NaCl), 3 times. Finally, the resulting MNPs were incubated with E-cad EC1-2 fragments at different ratios. When imidazole was used, the concentration was 0.25 M. Samples were centrifuged for 2h, 24,700 xg, 4 ºC.

3.3.3. Bradford assay[54]

To analyse the amount of protein present in the supernatants after incubation of MNPs with E-cad, the Bradford assay was performed. 150 μL of the sample were mixed with 150 μL of the Bradford reagent, agitated and incubated for 10 min at room temperature. Then, the absorbance was measured at 595 nm. All samples were measured in duplicate and, if possible, triplicate.

4. Results and discussion

4.1. E-cadherin (EC1-2) expression and purification

E-cadherin fragments were expressed in *E. coli* BL21 strains and purified as detailed in the experimental section. The obtained pellet of bacteria was 3 g. When purified, the cadherin fragments were immobilized in agarose beads presenting NTA-Ni^{2+} on the surface. As the E-cad fragments presented a His-tag, they were retained on the beads. When the protein was eluted for the first time, the ratio protein/beads was determined: around 1 mg protein per mL of beads. This meant that the protein obtained was 20 mg (for 3 g of pellet, in 500 mL of culture).

The protein is expressed inside the bacteria in form of inclusion bodies. Therefore, to purify them they were denaturalized and re-naturalized again, which is a sensitive process. To ensure that the folding was correct after purification, a trypsin sensitivity assay was performed. When the E-cad fragments are correctly folded, they are resistant to trypsin cleavage in presence of Ca^{2+} ions. However, they are sensitive to the cleavage without the calcium.[52] Figure 3 shows the results when the samples were loaded in SDS-PAGE. Both untreated and treated with trypsin in presence of Ca^{2+} samples showed a single band corresponding to the E-cad fragments. However, the sample treated with trypsin and EDTA (that chelates the metal ions and therefore withdraw Ca^{2+} from the media) was cleaved. These results confirm the correct folding of the protein. Furthermore, the SDS-PAGE reflects the high purity of the protein, as no bands are present but a single band with the expected size of the fragments (37 kDa) in lane 1.

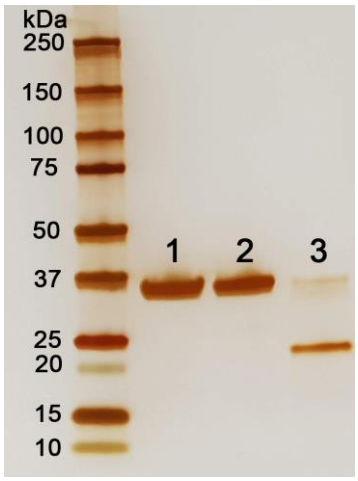

Figure 3. SDS-PAGE of the samples from the trypsin sensitivity assay. (1) Untreated E-cad fragment. (2) E-cad fragment treated with trypsin in presence of Ca^{2+}. (3) E-cad fragment treated with trypsin in presence of EDTA.

4.2. Water transfer of MNPs

Spherical MNPs of a diameter of 12 nm were used for this work. They were previously synthesized by Dr. Vanessa Herrero by thermal decomposition method, and their size and morphology characterized by TEM (see Annex I). However, the MNPs provided were not water soluble, as this synthesis technique provides of MNPs dispersed in organic media – hexane – and therefore they must be transformed to become water soluble, a requisite for most biological applications. Thus, before starting to optimize their oriented functionalization with E-EC1-2 cadherin, it was necessary to perform a water transference step using poly(maleic anhydride-*alt*-1-octadecene) (PMAO) as a coating agent (Figure 4). The conditions used were previously optimized in our.[32,53] PMAO is an amphiphilic polymer with hydrophobic alkyl chains that intercalate between the oleate molecules on the MNP surface. On the other end, PMAO has anhydride groups that can be hydrolysed in basic media, leaving free carboxyl groups that will have two main purposes: to stabilize the MNPs in aqueous media, and provide reactive groups for further functionalizations. In addition, before the hydrolysis of the anhydride groups, the polymer was previously modified with a fluorescent probe, tetramethylrhodamine-cadaverine (TAMRA). Thus, the coating step renders not only water soluble MNPs with a high yield (always between 75-100%), but fluorescent MNPs that facilitate future cell-nanoparticle interaction studies.

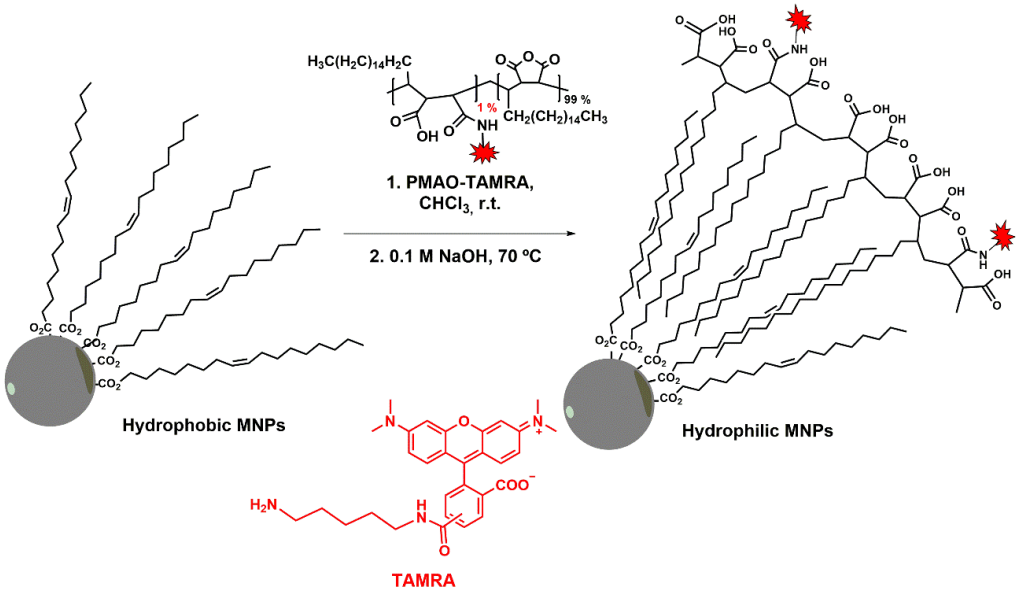

Figure 4. Scheme of the water transfer process with the PMAO-TAMRA (1%) polymer. On the left, MNPs in organic media with oleate coating. On the right, MNPs coated with the polymer through hydrophobic interactions between aliphatic chains and with the anhydride groups of PMAO hydrolysed. The structures of the polymer and the fluorophore are shown.

Once the process was completed, the polymer excess was removed with four washes consisting in ultracentrifugation steps. With an agarose gel electrophoresis, the correct elimination of the excess of polymer was confirmed by loading the purified MNPs (Figure 5, lanes 1-3) and the supernatants from each washing step (Figure 5, lanes 4-7). As shown in Figure 5b the polymer, fluorescent under UV light exposure, is completely removed after the fourth wash. Besides, Figure 5a compares the electrophoretic mobility of different batches of water transferred MNPs with that of previous transfers from the same magnetic core synthesis. The identical mobility indicates the correct water transfer of the MNPs, as well as the high reproducibility of the method.

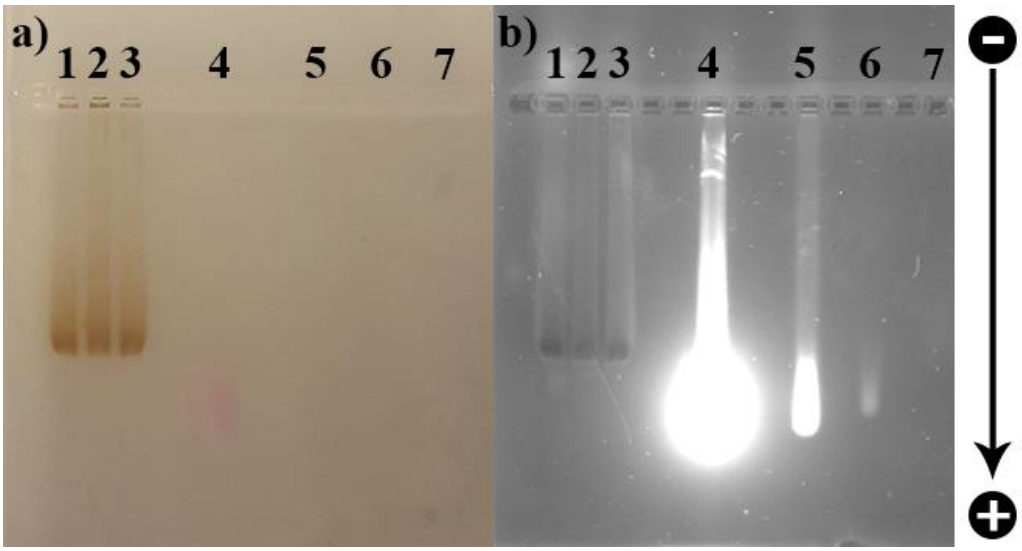

Figure 5. Agarose gel (1% m/v) electrophoresis of water transferred MNPs and washes' supernatants. (a) Visible light picture. (b) UV light illuminated picture. (1) Reference MNPs, previously transferred; from the same organic batch. (2, 3) Water transferred MNPs. (4, 5, 6, 7) Supernatants of successive washing steps.

For further characterization, a thermogravimetric analysis (TGA) was performed. This technique reveals the mass loss of a sample as the temperature increases (Figure A2). Therefore, information about the organic layers (oleate and polymeric coating) can be obtained. Oleate represented 12.1% of the total mass, whereas the PMAO reached almost 30%. With this data, available, the number of carboxyl groups present on the MNPs surface could be estimated to be around 4,000 carboxyl groups per nanoparticle (calculations are detailed in Annex II).

4.3. Dual functionalization approach of the MNPs: passivation and functionalization with NTA-Cu^{2+}

The next step was to optimize the functionalization of the PMAO-TAMRA nanoparticles with two functionalities: (1) NTA-Cu^{2+}, that will permit the further union of a His-tagged protein (E-cadherin, in this case) through its histidine tag; and (2) polyethylene glycol (PEG) or TRIS molecules to improve the colloidal stability of the MNPs.

Carbodiimide chemistry was elected to functionalize the MNPs. Carboxyl groups from the nanoparticles surface can react with amine groups present on the molecules to be attached. However, carboxyl groups must be activated with 1-ethyl-3-(3-dimethylaminopropyl)carbodiimide (EDC). Although it is a highly common reaction in organic chemistry, it is quite complex when used in nanotechnology due to possible side reactions, especially the hydrolysis of the resulting active intermediate *O*-acylisourea. The pH is key for the yield of the reaction: the amine group of the molecule has to be deprotonated (higher pH), but the carboxyl activation is more efficient at slightly acidic pH. The addition of N-hydroxysulfosuccinimide (S-NHS) stabilizes the active intermediate. Figure 6 represents the main pathways of the EDC chemistry.

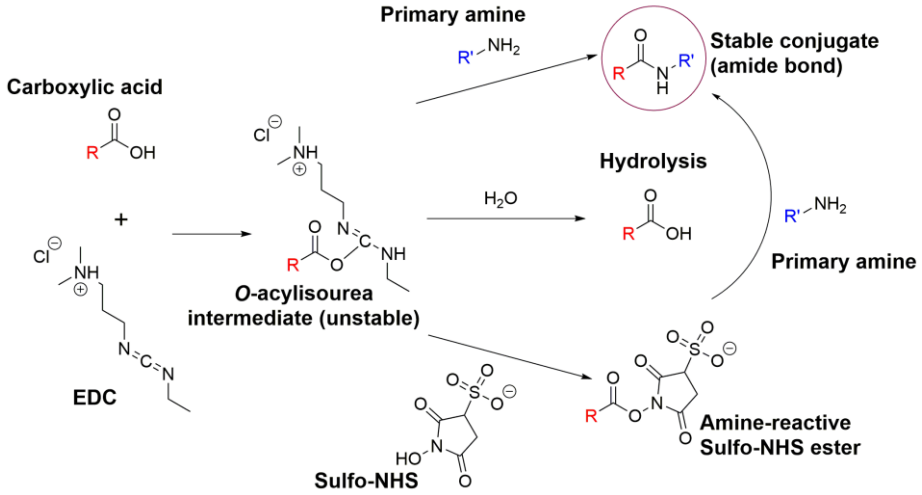

Figure 6. Activation of carboxyl groups with EDC chemistry. Formation of the desired amide bond (circled) and the possible side reactions.

In this work, two different molecules need to be bound on the MNPs surface. If both were added simultaneously while the carboxyl groups are activated, they would compete to react. Therefore, a sequential addition is necessary for a better control of the functionalization. The first approach (Strategy A) consisted on the activation of the carboxyl groups with EDC/S-NHS in acidic media, addition of the NTA-Cu^{2+} complex,

and subsequent blocking of the remaining activated groups with the passivating molecule (TRIS or different PEG molecules). The second approach (Strategy B) included two activation steps: one for the addition of PEG, and the other to functionalize with NTA-Cu^{2+}. The latter strategy was performed in alkaline media and with high excess of EDC. Figure 7 summarizes both protocols followed to functionalize the MNPs, and a more detailed explanation is then provided.

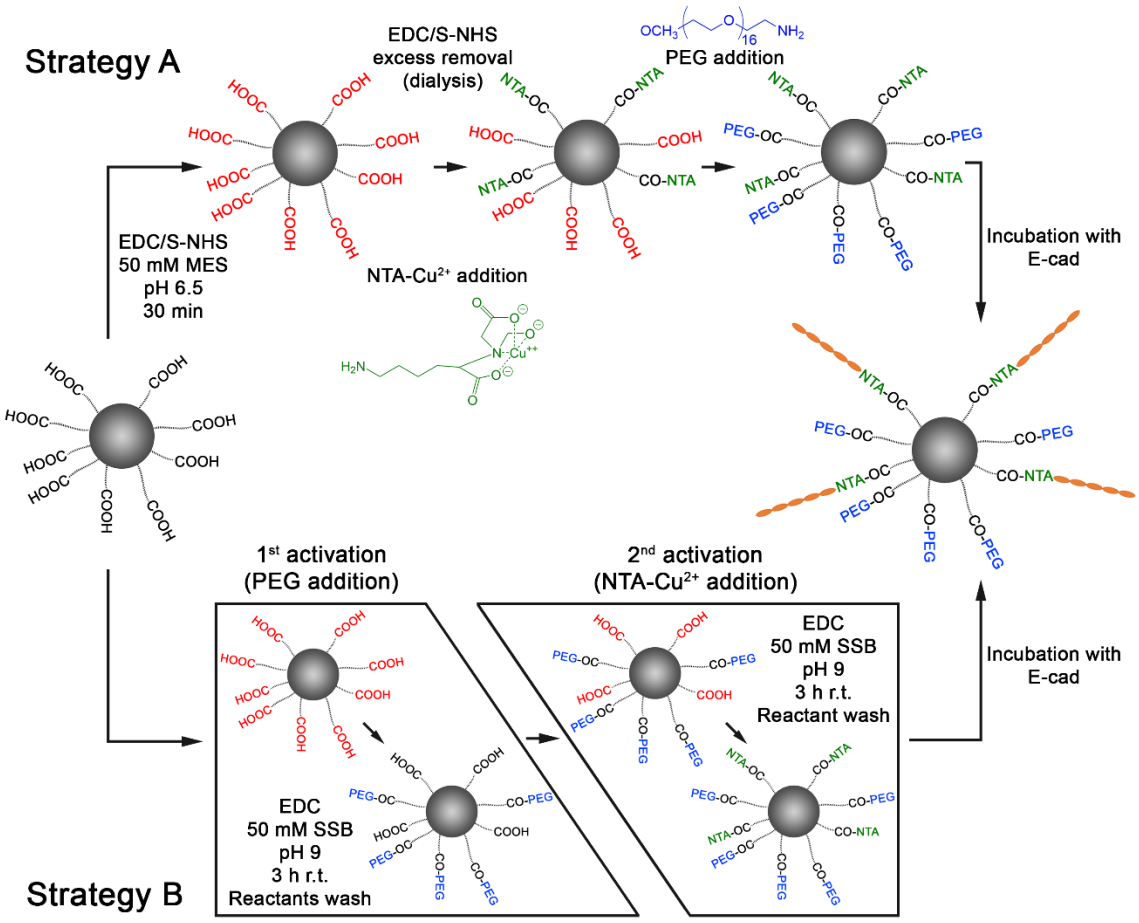

Figure 7. Scheme of the two strategies followed to functionalize MNPs with NTA-Cu^{2+} and to passivate them. In red, the carboxyl groups activated by the carbodiimide. PEG 750 Da is used to illustrate this scheme. All the passivation molecules were tested through "Strategy A".

4.3.1. Strategy A

The first strategy proposed (Figure 7, upper part) consisted on a first functionalization of MNPs with NTA-Cu^{2+} complex; the surface of the MNPs is afterwards passivated with different passivation molecules containing a primary amine group. The complete protocol can be found in the experimental section. Briefly, MNPs were incubated with EDC/S-NHS in a slightly acidic buffer to activate the carboxyl groups of the surface. The reaction intermediate is relatively more stable at this pH. After activation,

EDC/S-NHS excess was removed via dialysis in order to avoid side reactions of NTA. Then, the NTA-Cu^{2+} complex was added to the activated nanoparticles – the amount calculated to functionalize 30% of the carboxyl groups. Finally, the remaining activated groups on the MNPs surface were blocked with different molecules: TRIS and CH_3O-PEG-NH_2 with different molecular weights (750, 2000 and 5000 Da).

4.3.1.1. Incubation with E-cad

MNPs functionalized following *strategy A* were incubated with increasing ratios of E-cad and then centrifuged. The union was quantified by an indirect method, comparing the amount of E-cad on the supernatants with the amount of E-cad in the original solution. Quantification was performed by denaturizing polyacrylamide gel electrophoresis (SDS-PAGE) (Figure 8) followed by image analysis (using ImageJ software) and Bradford assay[54]. For a first trial, only MNPs passivated with TRIS were used.

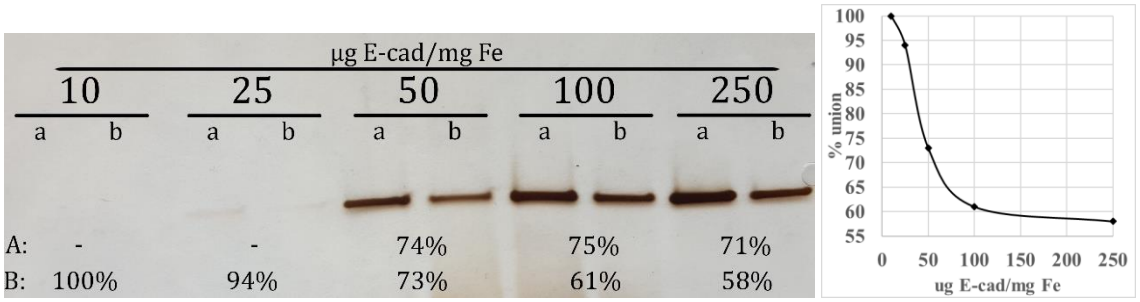

Figure 8. On the left, silver stained SDS-PAGE of different E-cad/MNPs ratio (from 10 to 250 µg E-cad/mg Fe), comparing the original E-cad solutions (a) and the supernatants after incubation (b). The union quantification was determined by image analysis with ImageJ (A) and Bradford assay (B). On the right, saturation curve of the E-cad union (% union vs. E-cad/MNPs ratio) based on the Bradford results.

The results show a clear difference between E-cad concentration in the original solution and the supernatants after the incubation with the NTA-Cu^{2+}-functionalized MNPs. The SDS-PAGEs were stained with the silver staining protocol. Although it is convenient for low protein amounts due to its low detection limit, silver staining is not the best technique to quantify different protein amounts, for the optimal revealing time for certain concentrations often results in under- or overexposure for others. That is why the 10 and 25 µg cad/mg Fe conditions could not be observed nor analysed, and the 100 and 250 cad/mg Fe conditions were overexposed and saturated and the ratio obtained by image analysis is not precise nor reliable. However, the image allows to determine qualitatively the union of the E-cad that is confirmed and more precisely quantified by the Bradford assay. With these data, a saturation curve can be drawn (Figure 8, right),

which shows that near the 100 μg E-cad/mg Fe ratio the MNPs do not accept more protein.

After those preliminary results, the four different batches of MNPs – each passivated with a different molecule of those mentioned before – were compared in terms of union efficiency. 50 μg E-cad/mg Fe were used for all cases. In addition, for the E-cad to be attached in an oriented manner, the functionalization should occur via chelation effect, and no other non-specific unions. To prove that, a new condition was added: all MNPs were also incubated with E-cad in the presence of imidazole (0.25 M), a well-known competitor of histidine in the chelation equilibrium with divalent metals (Cu^{2+}, Ni^{2+}, Co^{2+}).[48]

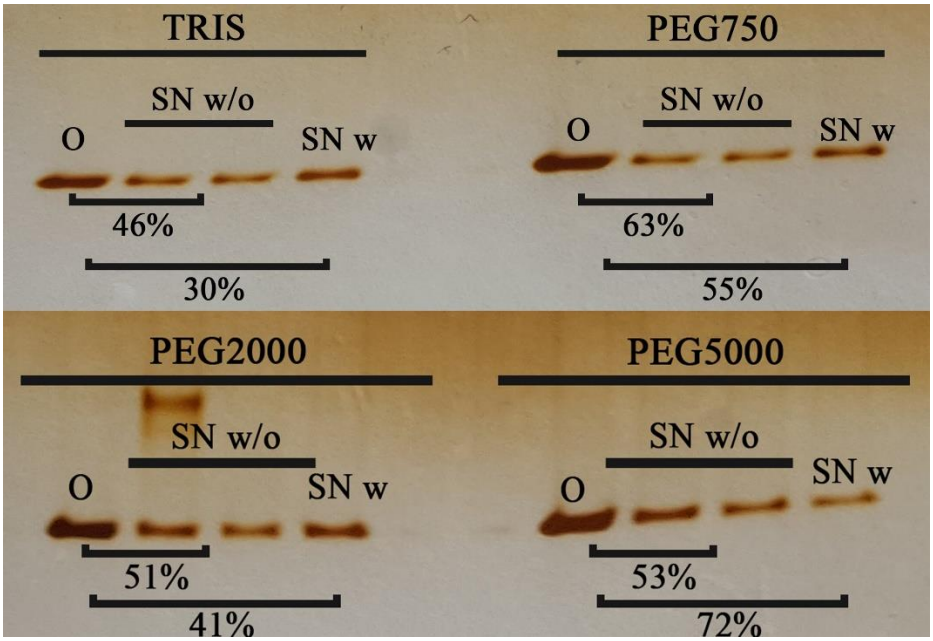

Figure 9. Silver stained SDS-PAGE of the original solutions of E-cad (O) and the supernatants after its incubation with MNPs passivated with different molecules (TRIS, PEG750, PEG2000, PEG5000) with (SN w) or without (SN w/o) imidazole 0.25 M. The union percentages were obtained by image analysis.

The results shown in Figure 9 reflect in all cases a significant union percentage of the protein in all four cases. Besides, the addition of imidazole reduced that union except for the PEG5000-passivated MNPs. This is not what was expected, as imidazole was supposed to impede the union of the E-cad in all cases, and more dramatically – in the best of the cases, there was only a 16% reduction on the binding efficiency. It should be taken into account that silver staining is a very sensitive developing technique, and minimum variations and errors can influence the result. Besides, as mentioned before, the revealing time can be crucial in case the gel bands saturate. A Bradford assay would be

needed to check these data, but for this particular experiment the samples were no longer available. However, although it cannot be quantified in a precise way, it can be clearly seen that a non-specific binding of cadherin fragments is competing with the affinity binding through metal chelation. This deficient functionalization is probably due to the deactivation of the carboxyl groups. To remove the excess of EDC/S-NHS, a dialysis step is performed; this step takes several hours in which part of the active intermediates can be hydrolysed (see Figure 6). With a deficient blocking of the MNPs surface, many carboxyl groups would remain free, and that can cause a non-specific union through ionic interactions with high positive charge density zones of the E-cad fragments.

This inefficiency in blocking the remaining carboxyl groups was also confirmed by a stability assay with culture media both with and without serum (fetal bovine serum, FBS), and the results are shown in Annex III (Figure A3). MNPs were incubated with the different media in 1:1 and 1:3 MNP:media volume ratios. Only the 1:3 ratio is shown.

The results show a clear aggregation for all cases when mixed with culture media (Dulbecco's Modified Eagle's Medium, DMEM) without FBS. DMEM is more complex than simple buffers, and presents a higher ionic strength. Thus, a bad passivation of the COOH groups can lead to a loss of a negative net charge of the nanoparticles, losing the repulsion and favouring the aggregation. When incubated in the presence of FBS, the stability of the MNPs increased dramatically independently of the passivating agent. This is most probably due to the formation of the protein corona, a mixture of proteins that absorb to the MNPs surface unspecifically due to ionic adsorption to the exposed carboxyl groups at the MNPs surface.[53] Although this protein corona clearly improves the colloidal stability of the E-cad, it might interfere in the future application of the functionalized MNPs, blocking sterically the interaction between the E-cad on the MNPs surface and the E-cad on the cell membranes. Besides, the formation of the corona indicates a deficient passivation of the surface. Considering that one of the passivation agents – PEG 750 Da – has been already used in our group and showed a great stabilization in MNPs with the same characteristics,[32] the protocol used in *Strategy A* is clearly not optimal. Therefore, a different strategy was designed, improving some technical aspects of the protocol.

4.3.2. Strategy B

Considering the results of the previous approach, the conditions were optimized in *strategy B* (Figure 7, lower part): (1) only PEG 750 Da was used as passivation agent for simplicity purposes, as it had resulted successful in previous works of the group; (2) the pH was raised to 9, closer to the pK_a of NTA and PEG, increasing the number of deprotonated amine groups, and therefore the molecules able to react; (3) diminish the deactivation of carboxyl groups eliminating the removal of the EDC excess. This step is common with biomolecules that present carboxyl and amine groups simultaneously – to avoid crosslinking. However, this PEG does not have a carboxyl groups, and those of the NTA molecule are protected as long as they are chelating the metal ion. A more detailed description is provided in the experimental section.

To further ensure that every step was successful, an agarose gel was loaded with the water transferred MNPs, the MNPs passivated with PEG, and the ones with NTA-Cu^{2+} (Figure 10). As each functionalization step implies the reaction of carboxyl groups, the electrophoretic mobility decreases, for the surface charge is less and less negative after each step. It is clear then that the functionalization is correct in both steps, and therefore the MNPs have now both the passivating molecule and the linker that will allow the oriented functionalization of the E-cad.

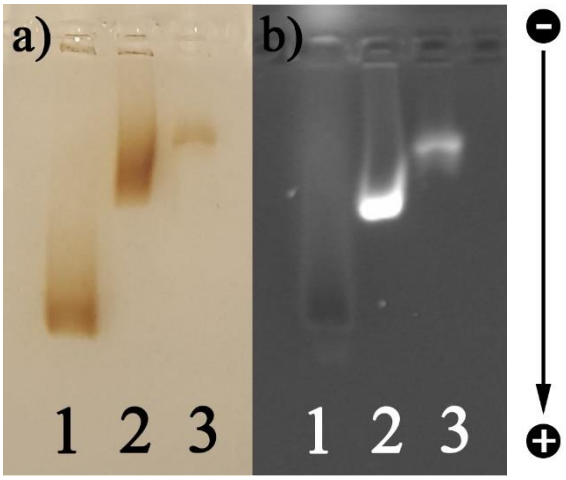

Figure 10. Agarose (1% m/v) gel of the different functionalization steps. (a) Visible light picture. (b) UV light illuminated picture. (1) Water transferred MNPs. (2) MNPs passivated with PEG 750. (3) MNPs passivated with PEG 750 and functionalized with NTA-Cu^{2+}.

4.3.2.1. Incubation with E-cad

The functionalization strategy was completely different and therefore so was the protocol, so firstly a new optimization of the E-cad:MNPs ratio was performed. Similarly to the previous case, the amount of E-cad was quantified by image analysis and Bradford assay (Figure 11). In both cases, the original E-cad solution was analysed and compared with the supernatants of the MNPs incubated with it. The results indicate the correct functionalization of the MNPs with E-cad when incubated with the 50 and 100 μg E-cad/mg Fe ratios. Nevertheless, there are more results worth analysing.

When incubated with 25 μg E-cad/mg Fe, there is negligible union of protein to the MNPs. The amount of protein present in these samples is very low, and the error could be high enough not to show significant differences – it should be noted that the absorbance of this particular sample in the Bradford assay is comparable to the blank. The next remarkable aspect is the quantification of the union in the presence of imidazole. In the SDS-PAGE, it seems to be more protein in the supernatant than in the original solution, which is obviously impossible. This experiment should be repeated to evaluate this observation. However, the Bradford assay shows more logical results. A 9% union of the E-cad compared with the 74% with the same protein amount without imidazole demonstrate that the linkage of the protein takes place through the chelation between the Cu^{2+} and the histidine tag, and unspecific binding of E/EC1-2 fragments was now avoided through an efficient passivation.

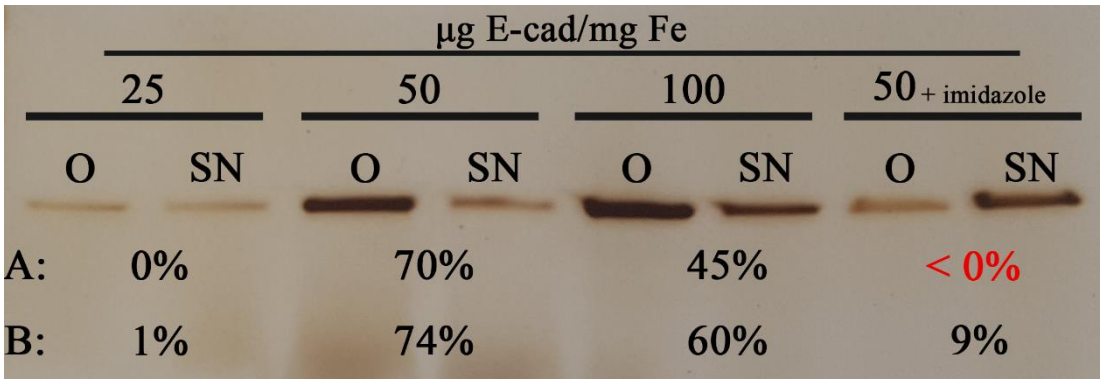

Figure 11. SDS-PAGE of different E-cad/MNPs ratio (from 25 to 100 μg E-cad/mg Fe), comparing the original E-cad solutions (O) and the supernatants after incubation (SN). The union quantification was determined by image analysis with ImageJ (A) and Bradford assay (B). An additional condition was quantified, with the E-cad remaining from the incubation of the MNPs in the presence of imidazole.

With the data obtained in this experiment, the number of E-cad molecules per nanoparticle was estimated. The sample with the 25 μg E-cad/mg Fe ratio could be analysed.

For the 50 and 100 μg E-cad/mg Fe, the mean was 3 and 4.6 molecules per nanoparticle. These results should be improved. For future interaction with cell membranes, to achieve a multivalent attachment, the number of protein fragments per nanoparticles should be higher. An increase of the NTA-Cu^{2+} groups or the use of bigger nanoparticles could solve the problem.

Finally, dynamic light scattering (DLS) and ζ-potential were measured for each functionalization step of *strategy B* (Table 1). The hydrodynamic diameters obtained for each sample were of the same order of magnitude, with small variations caused by the modification of the surface. The standard deviation is low in all cases, and the polydispersity index is below 0.3 for all samples, which indicated that they were not highly aggregated. It is crucial to achieve a correct functionalization and passivation to avoid aggregation because, in addition to alter the contact area, the physical properties can also be changed (i.e. the heating efficiency). As for the ζ-potential, the results of the three first samples are consistent with the agarose electrophoresis: in each functionalization step, more carboxyl groups have reacted with molecules, and therefore the net negative charge decreases. The consequent decrease of the ζ-potential when adding the cadherin fragments is consistent, as the net charge of the protein is negative at the pH in which the samples were measured: around 6.5 (theoretical isoelectric point of the fragments: 4.37).

Sample	Hydrodynamic diameter (nm)	ζ-potential (mV)
MNPs@PMAO	136 ± 14	-38 ± 1
MNPs@PMAO@PEG	111 ± 6	-20 ± 2
MNPs@PMAO@PEG@NTA-Cu^{2+}	138 ± 11	-4 ± 1
MNPs@PMAO@PEG@NTA@E-cad	120 ± 4	-14 ± 1

Table 1. Measurements of DLS and ζ-potential of the different functionalization steps followed in strategy B. Data from DLS given as intensity.

5. Conclusions

Magnetic nanoparticles, and especially iron oxide nanoparticles, have awakened great interest in different research fields due to their different properties – biocompatibility, stability. The biomedical applications of MNPs are more and more numerous day by day, with a special focus in cancer treatment or drug delivery. In this work, we sought the modification of these nanoparticles with the aim to attach them to the cell membrane. This would allow a new tool for many different applications in hyperthermia, biophysical studies, universalized transfection, etc.

The adhesion protein E-cadherin was selected as a targeting probe for the MNPs, taking advantage of its homologue interaction and ubiquity in epithelial cells. In order to increase the efficiency of union, the strategy of functionalization was designed to control the orientation of the protein to ensure a multivalent union with the cadherins, otherwise difficult due to the small effective contact area.

MNPs prepared through thermal decomposition method were successfully transferred to water in order for them to be water-soluble. This step, involving the coating with PMAO polymer, provided the surface of the nanoparticles with carboxyl groups that will allow further functionalizations. The approach to attach the E-cad in an oriented manner was to use NTA-Cu^{2+} to chelate a His-tagged recombinant E-cad (EC1-2). Two strategies were followed (A and B). Strategy A, consisting on a first functionalization with NTA-Cu^{2+} using EDC chemistry and the following blocking of the remaining activated groups with different passivating agents showed promising results in terms of functionalization, but regarding the MNP colloidal stability in physiological media. Strategy B used a protocol to obtain stable PEG (750 Da) functionalized MNPs as a first step. Then, the remaining carboxyl groups were again activated to functionalize the surface with NTA-Cu^{2+}. That functionalization was successful, and the incubation with E-cad revealed a good incorporation of the protein, with fair efficiencies at 50 and 100 μg E-cad/mg Fe ratios.

Lastly, the mechanism of union of the protein was determined. For the E-cad to be oriented, it should have been bonded via chelating effect of the Cu^{2+} with the His-tag. Imidazole was used as a competitor of the interaction between the divalent cation and the protein. In the case of Strategy A, the results were inconclusive and, although it showed less union efficiency with MNPs functionalized with three different passivation

agents, that efficiency surprisingly increased with MNPs coated with PEG 5000 Da. Regarding Strategy B, the addition of imidazole to the incubation mix highly decreased the interaction of the E-cad with the MNPs, therefore confirming a union via chelation. However, the theoretical calculation of number of E-cad fragments per nanoparticle reflects an insufficient functionalization for the future multivalent attachment to the cell membrane, an aspect that need further optimization.

6. Future perspectives

1. Stability assays of E-cad functionalized MNPs

Test the functionalized MNPs with DMEM with and without FBS to assess the stability in physiological media.

2. Cell culture assays: compare MDCK and Balb/c

To prove the biological activity of the platform here developed, different cell lines with distinct cadherin profile expressions should be incubated with the MNPs. In particular, MDCK cell line (dog kidney) expresses E-cadherin, while Balb/c (mouse hybridoma) does not. Therefore, the nanoparticles should theoretically attach to the former, but not to the latter. Besides, more studies could go in depth to the interaction MNPs-cells, such as the study with the W2A mutant, or the comparison with microbeads to study the effect of the contact area and cadherin density.

3. Time lapse studies: determine how long do MNPs stay on the membrane

By using the fluorescence of MNPs due to the TAMRA linked to the polymer, studies using a confocal microscope could determine the location of the MNPs at different times. In that way we could study the maximum time the MNPs can stay immobilized on the cell membrane.

4. Hyperthermia studies

Once the immobilization of the MNPs to the cell membrane is optimized, hyperthermia studies would be carried out. The cellular death by different mechanisms (apoptosis, necrosis, etc.) should be assessed, as well as the formation of transitory pores. The last objective could be studied by using probes of different sizes; evaluating which of them are able to pass the cell membrane would allow to determine the size of the pores that this system generates.

5. Future optimization

In case that future results fail, different parameters should be considered to improve. If the attachment to the membrane is not good, larger particles (50-80 nm) could increase the contact area and ease a multivalent interaction. Besides, different sizes and shapes of nanoparticles could be tested in order to obtain better heating efficiency, and therefore better generation of hotspots.

7. Bibliography

1 K. Riehemann, S. W. Schneider, T. A. Luger, B. Godin, M. Ferrari and H. Fuchs, *Angew. Chemie Int. Ed.*, 2009, **48**, 872–897.

2 E. Roduner, *Chem. Soc. Rev.*, 2006, **35**, 583.

3 F. U. Rehman, C. Zhao, H. Jiang and X. Wang, *Biomater. Sci.*, 2016, **4**, 40–54.

4 X. Wang, Y. Hu and H. Wei, *Inorg. Chem. Front.*, 2016, **3**, 41–60.

5 A. Samanta and I. L. Medintz, *Nanoscale*, 2016, **8**, 9037–9095.

6 D. He and J. Marles-Wright, *N. Biotechnol.*, 2015, **32**, 651–657.

7 M. Thiruvengadam, G. Rajakumar and I.-M. Chung, *3 Biotech*, 2018, **8**, 74.

8 L. Luo, R. Shu and A. Wu, *J. Mater. Chem. B*, 2017, **5**, 5517–5531.

9 A. Hervault, A. E. Dunn, M. Lim, C. Boyer, D. Mott, S. Maenosono and N. T. K. Thanh, *Nanoscale*, 2016, **8**, 12152–12161.

10 A. A. Bhirde, V. Patel, J. Gavard, G. Zhang, Ḱ. A. A. Sousa, A. Masedunskas, R. D. Leapman, Ḱ. R. Weigert, J. S. Gutkind and J. F. Rusling, *ACS Nano*, 2009, **3**, 307–316.

11 B. Lu, H. Ye, S. Shang, Q. Xiong, K. Yu, Q. Li, Y. Xiao, F. Dai and G. Lan, *Nanotechnology*, 2018, **29**, 425603.

12 M. Carrion-Vazquez, H. Li, H. Lu, P. E. Marszalek, A. F. Oberhauser and J. M. Fernandez, *Nat. Struct. Mol. Biol.*, 2003, **10**, 738–743.

13 S. Ruiz-Rincón, A. González-Orive, J. M. de la Fuente and P. Cea, *Langmuir*, 2017, **33**, 7538–7547.

14 J. Mosayebi, M. Kiyasatfar and S. Laurent, *Adv. Healthc. Mater.*, 2017, **6**, 1700306.

15 P. Sharma, S. Brown, G. Walter, S. Santra and B. Moudgil, *Adv. Colloid Interface Sci.*, 2006, **123**–**126**, 471–485.

16 M. Moros, B. Pelaz, P. López-Larrubia, M. L. García-Martin, V. Grazú and J. M. de la Fuente, *Nanoscale*, 2010, **2**, 1746.

17 S. F. Hasany, I. Ahmed, R. J and A. Rehman, *Nanosci. Nanotechnol.*, 2013, **2**, 148–158.

18 T. Kondo, K. Mori, M. Hachisu, T. Yamazaki, D. Okamoto, M. Watanabe, K. Gonda, H. Tada, Y. Hamada, M. Takano, N. Ohuchi and Y. Ichiyanagi, *J. Appl. Phys.*, 2015, **117**, 17D157.

19 J.-P. Fortin, F. Gazeau and C. Wilhelm, *Eur. Biophys. J.*, 2008, **37**, 223–228.

20 R. Kötitz, W. Weitschies, L. Trahms and W. Semmler, *J. Magn. Magn. Mater.*, 1999, **201**, 102–104.

21 E. Guisasola, L. Asín, L. Beola, J. M. de la Fuente, A. Baeza and M. Vallet-Regí, *ACS Appl. Mater. Interfaces*, 2018, **10**, 12518–12525.

22 M. Ohtake, M. Umemura, I. Sato, T. Akimoto, K. Oda, A. Nagasako, J.-H. Kim, T. Fujita, U. Yokoyama, T. Nakayama, Y. Hoshino, M. Ishiba, S. Tokura, M. Hara, T. Muramoto, S. Yamada, T. Masuda, I. Aoki, Y. Takemura, H. Murata, H. Eguchi, N. Kawahara and Y. Ishikawa, *Sci. Rep.*, 2017, **7**, 42783.

23 R. A. Revia and M. Zhang, *Mater. Today (Kidlington).*, 2016, **19**, 157–168.

24 G. R. Iglesias, A. V. Delgado, F. González-Caballero and M. M. Ramos-Tejada, *J. Magn. Magn. Mater.*, 2017, **431**, 294–296.

25 X. Li, J. Wei, K. E. Aifantis, Y. Fan, Q. Feng, F. Z. Cui and F. Watari, *J. Biomed. Mater. Res. - Part A*, 2016, **104**, 1285–1296.

26 L. Asín, G. Stepien, M. Moros, R. M. Fratila and J. M. de la Fuente, in *Clinical Applications of Magnetic Nanoparticles*, ed. N. T. K. Thanh, CRC Press, 1st edn., 2018, pp. 305–317.

27 D. Chang, M. Lim, J. A. C. M. Goos, R. Qiao, Y. Y. Ng, F. M. Mansfeld, M. Jackson, T. P. Davis and M. Kavallaris, *Front. Pharmacol.*, 2018, **9**, 831.

28 L. Arias, J. Pessan, A. Vieira, T. Lima, A. Delbem and D. Monteiro, *Antibiotics*, 2018, **7**, 46.

29 R. Di Corato, A. Espinosa, L. Lartigue, M. Tharaud, S. Chat, T. Pellegrino, C. Ménager, F. Gazeau and C. Wilhelm, *Biomaterials*, 2014, **35**, 6400–6411.

30 J. D. Byrne, T. Betancourt and L. Brannon-Peppas, *Adv. Drug Deliv. Rev.*, 2008, **60**, 1615–1626.

31 H. Koo, M. S. Huh, I.-C. Sun, S. H. Yuk, K. Choi, K. Kim and I. C. Kwon, *Acc. Chem. Res.*, 2011, **44**, 1018–1028.

32 R. M. Fratila, M. Navascuez, J. Idiago-López, M. Eceiza, J. I. Miranda, J. M. Aizpurua and J. M. de la Fuente, *New J. Chem.*, 2017, **41**, 10835–10840.

33 J.-L. Maître and C.-P. Heisenberg, *Curr. Biol.*, 2013, **23**, R626–R633.

34 M. Takeichi, *Curr. Opin. Cell Biol.*, 1995, **7**, 619–627.

35 M. P. Stemmler, *Mol. Biosyst.*, 2008, **4**, 835.

36 Y. Ma, H. Zhang, C. Xiong, Z. Liu, Q. Xu, J. Feng, J. Zhang, Z. Wang and X. Yan, *Cancer Lett.*, 2018, **430**, 201–214.

37 H. Chen, X. Wang, Q. Zhou, P. Xu, Y. Liu, M. Wan, M. Zhou and C. Mao, *Langmuir*, 2017, **33**, 13430–13437.

38 R. Chaudhary, K. Roy, R. K. Kanwar, R. N. Veedu, S. Krishnakumar, C. H. A. Cheung, A. K. Verma and J. R. Kanwar, *Aust. J. Chem.*, 2016, **69**, 1108.

39 M. Moros, F. Delhaes, S. Puertas, B. Saez, J. M. de la Fuente, V. Grazú and H. Feracci, *J. Phys. D. Appl. Phys.*, 2016, **49**, 054003.

40 F. van Roy and G. Berx, *Cell. Mol. Life Sci.*, 2008, **65**, 3756–3788.

41 E. Perret, A.-M. Benoliel, P. Nassoy, A. Pierres, V. Delmas, J.-P. Thiery, P. Bongrand and H. Feracci, *EMBO J.*, 2002, **21**, 2537–2546.

42 S. Chevalier, C. Cuestas-Ayllon, V. Grazu, M. Luna, H. Feracci and J. M. De La Fuente, *Langmuir*, 2010, **26**, 14707–14715.

43 R. B. Troyanovsky, O. Laur and S. M. Troyanovsky, *Mol. Biol. Cell*, 2007, **18**, 4343–4352.

44 Y. Wu, P. Kanchanawong and R. Zaidel-Bar, *Dev. Cell*, 2015, **32**, 139–154.

45 R. M. Fratila, S. G. Mitchell, P. del Pino, V. Grazu and J. M. de la Fuente, *Langmuir*, 2014, **30**, 15057–15071.

46 K. J. Petty, in *Current Protocols in Molecular Biology*, John Wiley & Sons, Inc., Hoboken, NJ, USA, 2001, pp. 10–24.

47 E. Hochuli, W. Bannwarth, H. Döbeli, R. Gentz and D. Stüber, *Nat. Biotechnol.*, 1988, **6**, 1321–1325.

48 S. Knecht, D. Ricklin, A. N. Eberle and B. Ernst, *J. Mol. Recognit.*, 2009, **22**, 270–279.

49 C. Kim, J. F. Galloway, K. H. Lee and P. C. Searson, *Bioconjug. Chem.*, 2014, **25**, 1893–1901.

50 C. Li, G. Wu, R. Ma, Y. Liu, Y. Liu, J. Lv, Y. An and L. Shi, *ACS Biomater. Sci. Eng.*, 2018, **4**, 2007–2017.

51 D. Keller, A. Beloqui, M. Martínez-Martínez, M. Ferrer and G. Delaittre, *Biomacromolecules*, 2017, **18**, 2777–2788.

52 O. Courjean, G. Chevreux, E. Perret, A. Morel, S. Sanglier, N. Potier, J. Engel, A. van Dorsselaer and H. Feracci, *Biochemistry*, 2008, **47**, 2339–2349.

53 G. Stepien, M. Moros, M. Pérez-Hernández, M. Monge, L. Gutiérrez, R. M. Fratila, M. de las Heras, S. Menao Guillén, J. J. Puente Lanzarote, C. Solans, J. Pardo and J. M. de la Fuente, *ACS Appl. Mater. Interfaces*, 2018, **10**, 4548–4560.

54 M. M. Bradford, *Anal. Biochem.*, 1976, **72**, 248–254.